Effect of Strain on the Resistivity and Thermal Conductivity of High Purity Niobium

S. Balachandran, P. Xu, P. Dhakal, M. Carl, R. P. Walsh, and P. J. Lee, *Senior Member, IEEE*

***Abstract*—High purity niobium (Nb) is a technologically important material for large-scale accelerator and nano-scale quantum computing applications in microwave frequency range. The high thermal conductivity and low resistivity of Nb are critical to the high performance at temperature range of 0.01–4.0 K. The presence of interstitials such as O, N, H, and C act as scattering centers and alter the mean free path, reducing resistivity and thermal conductivity, and contributing significantly to Nb's thermal performance for temperatures of 2.0 K and above. The residual resistivity ratio (RRR), defined as the ratio of the normal state resistivity at 300 K to that at 4.2 K (Nb, $T_c = 9.2$ K), is an accepted direct estimate of the impurity content of fully recrystallized Nb. Complete re-crystallization of Nb is challenging unless very high temperatures are employed, which is often impractical, hence, in practice, dislocation and dislocation structures impact the thermal performance of Nb due to strong phonon scattering contributions. This paper reports on the degradation of thermal conductivity and RRR of high purity Nb large grain, single crystal with fixed impurity, varying strain, and dislocation content levels. Experimental thermal conductivity data fits the Boltzmann transport equation incorporating dislocation density.**

***Index Terms*—Thermal conductivity, niobium, superconducting radio frequency cavities.**

I. Introduction

NIOBIUM superconducting radio frequency (SRF) cavities are enabling technology for accelerators and beams [1]. The emerging area of quantum computing [2] Nb, being a metallic superconductor with a critical temperature (T_c) of 9.2 K, a lower critical magnetic field H_{c1} of 200 mT, and excellent bulk fabricability, provides a distinct advantage to fabricate complex cavity shapes [3]. High field gradients beyond 40 MV/m [4] and high efficiencies or quality factors ($Q_0 \sim 10^{10} - 10^{11}$) ($\sim$ 1.5-1.7 K) are obtainable with SRF Nb cavities with various methodologies of tuning the surface by interstitial doping and surface preparation [4], [5], [6], [7], [8]. The temperature range of operation of these SRF structures varies between mK (quantum computing and sensing) to 2.0 K (linear accelerators). At these low temperatures, thermal conductivity, κ of Nb is poor, and dissipation of heat due to RF losses could be a limiting issue for devices. Electron transport is largely diminished due to the formation of Cooper pairs below T_c, and the main mechanism that dominates thermal conductivity is the phonon transport [15]. Phonons can be disrupted by the following mechanisms: a) scattering due to normal unpaired electrons, b) boundary scattering, and c) due to crystalline defects such as dislocations of the crystal lattice. By far, most models for Nb adopt phonon scattered by electrons and boundaries to fit the $<$ 10 K data, however, considerations of dislocation based scattering are not common. The assumption to neglect dislocation based scattering can however be critical since Nb needs to be formed into complex shapes through deformation which leads to lattice defects in the form of dislocations and dislocation structures [9]. These defects cannot be easily annealed once formed [10], and will disrupt the low temperature thermal conductivity. Recently, Xu et al. [11], [12] have incorporated a microscopic model to include dislocation density (N_d) in the phonon-dislocation interaction term for κ. A dislocation based model can be explored by advanced microscopy techniques as well as careful uni-axial strain based systematic studies.

In this paper we provide a systematic preliminary study of thermal conductivity, in a large grain-single crystal undergoing permanent plastic to varying strain levels and we fit the model developed by Xu et al. [12]. With the initial material state being a constant, we are able to deduce the N_d and resistivity as a function of strain, ϵ. Our initial evaluations show that the model is robust for tracking variations in the material state such as heat treatments and changes in interstitials when heat treated, even when the dislocation content does not vary. These promising results suggest predictability of κ, in the presence of microscopic variables.

II. Materials and Methods

A. Description of Raw Material and Samples

The Nb used in this study is from a multiple-pass electron beam (EB) melted large grain ingot. The material chemistry

Manuscript received 14 November 2022; revised 4 March 2023; accepted 10 March 2023. Date of publication 27 March 2023; date of current version 10 April 2023. This work was supported in part by the U.S. DOE, Office of Science, Office of HEP under Grant DE-SC0009960, in part by NHMFL through NSF Cooperative Agreement under Grant DMR-1644779 and the State of Florida, and in part by Jefferson Science Associates, LLC under U.S. DOE Grant DE-AC05-06OR23177. *(Corresponding author: S. Balachandran.)*

S. Balachandran is with the National High Magnetic Field Laboratory, Florida State University, Tallahassee, FL 32309 USA, and also with the Thomas Jefferson National Accelerator Facility, Newport News, VA 23606 USA (e-mail: shreyas@jlab.org).

P. Xu, R. P. Walsh, and P. J. Lee are with the National High Magnetic Field Laboratory, Florida State University, Tallahassee, FL 32309 USA (e-mail: peng.xu@magnet.fsu.edu; walsh@magnet.fsu.edu; lee@asc.magnet.fsu.edu).

P. Dhakal is with the Thomas Jefferson National Accelerator Facility, Newport News, VA 23606 USA (e-mail: dhakal@jlab.org).

M. Carl is with ATI Metals, Albany, OR 97321 USA (e-mail: Matthew.Carl@ATImetals.com).

Color versions of one or more figures in this article are available at https://doi.org/10.1109/TASC.2023.3262218.

Digital Object Identifier 10.1109/TASC.2023.3262218

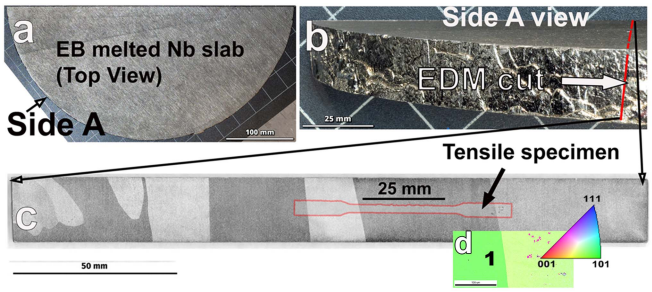

Fig. 1. Electron beam melted Nb slab of RRR ∼267 (measured at ATI) as received from ATI metals. a, and b indicate the different views of the slab, c, is the EDM'ed slab out of which sub-specimen tensile samples in accordance with ASTM-E8 were cut after an initial buffered chemical polish (BCP) of the Nb slab, and d, is the orientation imaging micrograph of grain 1, which is along the gage length of the tensile specimen.

is in accordance with high purity Nb for SRF applications, with interstitial content H, N, O $<$ 10 ppm. The RRR measured at Allegheny Technologies Incorporated (ATI) Metals was 267. Fig. 1(a) and (b) depicts the ingot slab, from which cross-sectional strips were cut with a wire electro-discharge machine (EDM) and chemically polished using a standard buffer chemical polish containing 1:1:2 of $HF : HNO_3 : H_3PO_4$ by volume to reveal the large Nb cast grains. A large grain bi-crystal was selected and ASTM-E8 [13] sub-specimen were cut with the gauge length of 30 mm, and thickness of ∼3 mm. In order to reduce the variables, the gauge length section of each of the specimen consisted of the same large grain. In all the tests performed, the orientation was kept a constant. Tensile tests were conducted in accordance to ASTM E8, under displacement control and a strain rate of $5 \times 10^{-5}\,\mathrm{s}^{-1}$. Strain was measured using a class E extensometer over a gauge length of 25 mm. The tensile deformation is given by the engineering strain ϵ, defined as: $\epsilon = (L_f - L_0)/L_0$, where L_f is the final length, and L_0 = 25 mm is the initial gauge length. The tensile samples were strained in the range of $\epsilon = 0.51$–16 %. All the tensile tests were conducted at NHMFL.

B. Thermal Conductivity Measurements

Experimental thermal conductivity measurements were performed at Jefferson Lab, using an in-house setup and procedures developed for measurement of thermal conductivity of Nb in the temperature range of 1.5 K–10 K as mentioned in [14]. The setup is immersed in liquid helium and lower temperatures were obtained by pumping the liquid helium to sub atmospheric pressure. A heater was installed at one end of the sample and the other end was exposed to superfluid helium.

In steady state, the thermal conductivity, κ of the specimen as a function of temperature (T) is given by

$$\kappa = \frac{Pd}{A\Delta T} \tag{1}$$

where P is the power supplied to the resistive heater, d is the distance between two temperature sensors installed on the specimen, $\Delta T = T_1 - T_2$ is the temperature difference between two temperature sensors and A is the cross-sectional area of the specimen.

III. Thermal Conductivity Model

The thermal conductivity of Nb modeled here is a parameterized approach of Bardeen- Rickayzen-Tewordt (BRT) [15], as performed by Koechlin and Bonin [16], according to the Bardeen-Copper-Schrieffer (BCS) theory [17]. A brief description of the model is as follows. Thermal conductivity is an additive effect of electron and phonon contributions and can be expressed as $\kappa = \kappa_e + \kappa_p$, where κ_e represents the thermal energy carried by electrons, and κ_p, the thermal energy carried by phonons. The thermal conductivity due to electrons is given by

$$\kappa_e = R(y)\left[\frac{\rho}{LT} + aT^2\right]^{-1} \tag{2}$$

where the term y in $R(y)$ is defined as, $y = \Delta(T)/k_BT$, where $\Delta(T)$ is the superconducting energy gap, k_B is the Boltzmann constant, ρ is electrical resistivity at 4.2 K. $L = 2.45 \times 10^{-8}\,W\mathrm{K}^{-2}$ is the Lorentz constant, and a is the coefficient of momentum exchange of electrons with the lattice. The term $R(y)$ quantifies the condensation of normal conducting electrons into Cooper pairs, $R(y) = 1$ at normal conducting state. The phonon contribution κ_p is given by,

$$\kappa_p = \left[\frac{1}{De^yT^2} + \frac{1}{BlT^3} + W_d\right]^{-1} \tag{3}$$

where D refers to phonon scattered by electrons, B corresponds to phonon scattered by boundary scattering, including physical or/and grain boundaries, l is the phonon mean free path, and W_d, is the thermal resistance due to phonon scattered by dislocations developed by Xu [12], which incorporates the randomly distributed dislocation structure as described by Klemens [18] as

$$\frac{W_dT^2}{N_d} = \frac{0.38\,vh^2b^2\gamma^2}{K_B^3} \tag{4}$$

where N_d is the dislocation density, γ is the Grüneisen constant (1.4 for Nb), b is the Burgers vector, v is the average group velocity of Nb, h is the Planck constant, and k_B is the Boltzmann constant. In the superconducting regime of interest, κ_e decreases due to the free electrons forming Cooper pairs, and the κ_p term dominates at very low temperatures. The experimental data is fit to determine the model parameters, a, D, B, N_d. Since we do not have an independent resistivity measurement we also fit ρ and report it here.

IV. Results

A. Tensile Testing

Fig. 2 shows the tensile testing done of the large grain EBM, as received (AR) Nb with a single crystal (labeled 1, in Fig. 1) in the gauge length. The orientation of this crystal in Euler angles is: ϕ_1= 323°, Φ = 53°, ϕ_2 = 186°, this corresponds to the tensile axis is along the [111] orientation of the crystal indicated by the inverse pole figure (IPF) insert in Fig. 2. For this study

TABLE I
SUMMARY OF MODEL PARAMETER FIT OF THE EXPERIMENTAL THERMAL CONDUCTIVITY DATA

Fitting parameters	As received (AR)	AR+ϵ=5.1%	AR+ϵ=10.2%	AR+ϵ=16%	AR+1000 °C/3 h
Dislocation density, N_d m^{-2}	1.21×10^{10}	6.74×10^{13}	2.34×10^{14}	8.1×10^{14}	1.19×10^{10}
Phonon-boundary scattering, B $Wm^{-2}K^{-4}$	451	451	451	451	6164
Phonon-electron scattering, D $Wm^{-1}K^{3}$	3×10^{-3}	3×10^{-3}	3×10^{-3}	3×10^{-3}	3×10^{-3}
Coeff. of electron-lattice momentum exchange, a $mW^{-1}K^{-1}$	3.9×10^{-6}	3.9×10^{-6}	3.9×10^{-6}	3.9×10^{-6}	3.9×10^{-6}
Resistivity at 4.2 K, $\mu\Omega cm$	4.3×10^{-2}	4.97×10^{-2}	5.15×10^{-2}	5.5×10^{-2}	7.16×10^{-2}
R^2-model fits to experimental data	0.949	0.999	0.997	0.996	0.999

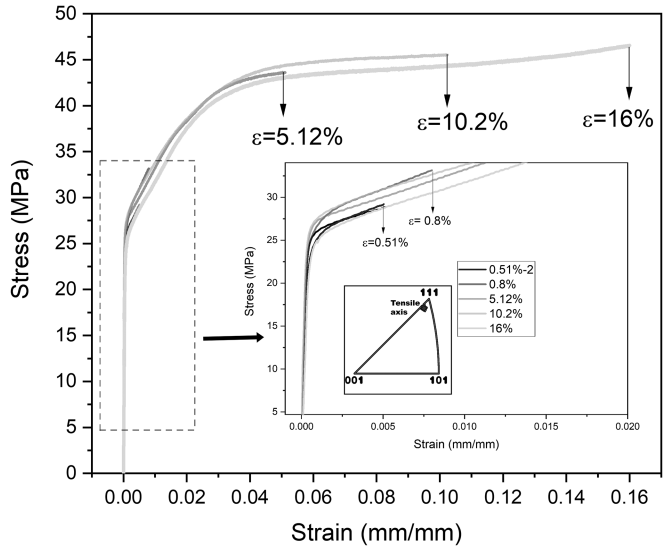

Fig. 2. Tensile test of all the large grain samples used in this study with a single grain in the gauge length deformed to various levels of plastic strain ϵ. The tensile axis corresponds to $\sim$ [111], as indicated in the IPF. Notice the considerable repeatability in the tensile test curves from different samples.

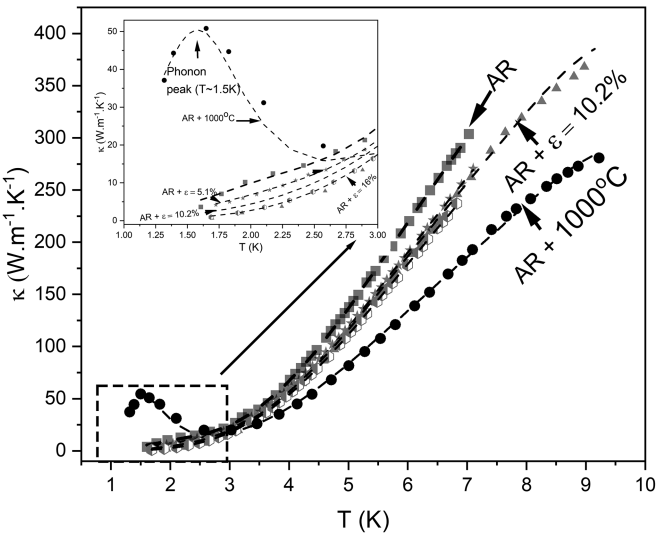

Fig. 3. Thermal conductivity as a function of temperature as obtained experimentally is shown by symbols. The dotted line corresponds to the model fit. The model as described in Section III, fits the experimental data well in the superconducting regime.

we stopped the tests on the various samples at strain values of 0.005, 0.008, 0.051, 0.102, and 0.16. The stress-strain response is consistent with high purity Nb, with very low initial yield strength value in the range of 26–29 MPa. The flow stress values at $\epsilon = 5$ %, 10 % and 16 % are 42.5 MPa, 45 MPa, and 45.3 MPa, respectively. Notice the higher slope in the low strain regime of $\epsilon < 5\%$, and a decreased slope after $\epsilon > 5\%$ for these samples. The consistent stress-strain response with minimal deviations suggests that samples have a similar initial starting condition which is important for comparisons.

B. Thermal Conductivity

Thermal conductivity measurements in the range of 1.5–10 K were performed on the AR, AR+$\epsilon = 0.05$, AR+$\epsilon = 0.102$, and AR+$\epsilon = 0.16$ samples. The experimental data along with the model fit are shown in Fig. 3. The parameters, N_d, B, D, a, and ρ for fits obtained are summarized in Table I.

The fitting process was performed in the following way: First, the AR sample was fitted with 5 parameters, then parameters a, B, and D were kept the same for the strained sample, only ρ and N_d were fitted. For the sample after heat treatment, the boundary scattering term B was fitted in addition to the parameters ρ and N_d.

The fit predicts an increase in the dislocation density with strain from an initial dislocation density of $1.2 \times 10^{10}\,\mathrm{m}^{-2}$ in the AR sample to $8.10 \times 10^{14}\,\mathrm{m}^{-2}$, after a strain of $\epsilon = 0.16$. After a 1000 °C/3 h heat treatment of the AR sample, no change in dislocation density is implied, however the heat treatment does increase the phonon-boundary scattering term by an order of magnitude to 6164. The model fits the contribution of phonon scattering by dislocations, and predicts the dislocation density. The plot of predicted dislocation density with strain in Fig. 4 shows a high increase in dislocation density during the initial deformation and a gradual leveling at higher strain values.

Since we did not measure the resistivity of the sample independently, we have predicted the resistivity from the thermal conductivity data. The $\rho_{4.2\,K}$ increases with strain from $4.3 \times 10^{-2}\,\mu\Omega \cdot \mathrm{cm}$ in the AR condition to $5.5 \times 10^{-2}\,\mu\Omega \cdot \mathrm{cm}$ after a deformation of $\epsilon = 0.16$. The model fit of ρ provides a prediction of variation in resistivity as a function of strain plotted as $\rho - \rho_{\epsilon=0}$ vs. ϵ, as shown in Fig. 5, and compared with data obtained by Zubeck [19] in the same strain range.

V. DISCUSSION

There is a clear indication from the experimental data in Fig. 3 that strain has a detrimental impact on the thermal conductivity. The model for thermal conductivity presented in Section III fits

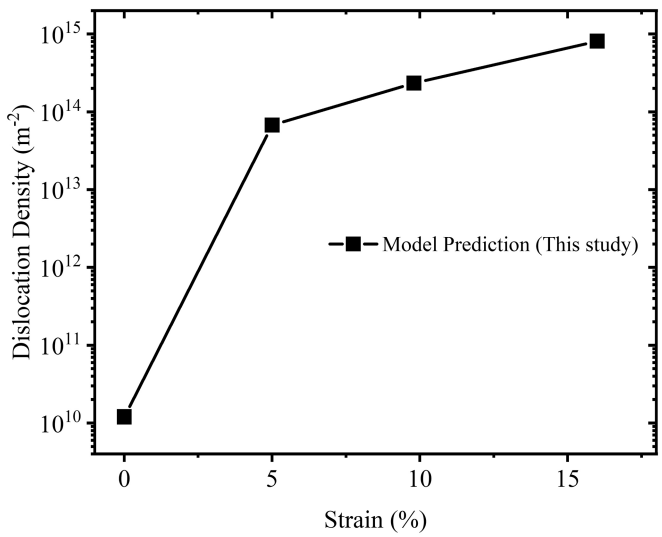

Fig. 4. Predicted dislocation density as a function of tensile strain. The model predicts an expected higher increase in dislocation density during initial stages of deformation and the gradual leveling off after subsequent straining.

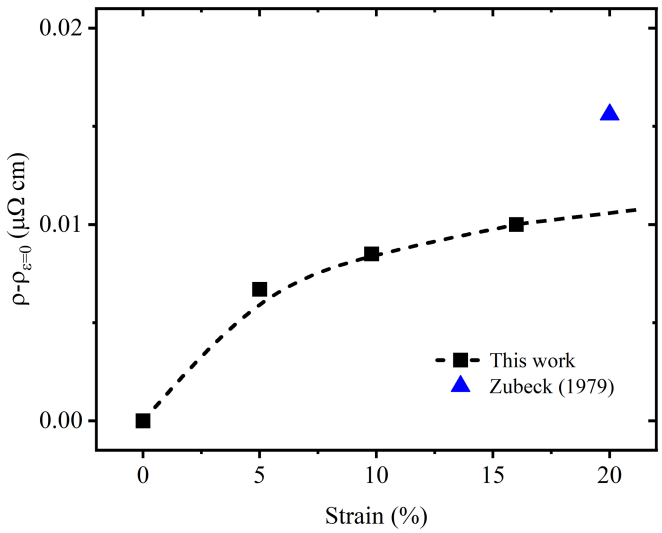

Fig. 5. Contribution to Nb resistivity as a function of tensile strain as predicted by the thermal conductivity model. The parabolic curve is added as a guide to the eye.

the thermal conductivity data with very high confidence. The fit parameters indicate that the phonons scattered by electrons and the electron scattered by phonons in Nb do not change during the course of the study. The major differences predicted by the model due to strain are in the electron resistivity term and the phonon-dislocation coupling component which leads to the prediction of dislocation density in the present model. There is also a variation in the boundary scattering term between the AR, AR + strained samples and the 1000 °C/3 h heat treated samples.

A. *Effect of Strain and Dislocation Density*

Based on the design of the experiment, the major differences that occur in the phonon-scattering terms are due to the increase in dislocation line defects with strain. Fig. 2 indicates the typical flow stress or resistance to deformation as the material is strained. The high initial slope of stress versus strain (large strain hardening) in the Nb sample (also known as stage 1, 2 hardening) occurs due to a high increase in the dislocation density [20], and the subsequent decrease in slope occurs when dislocations form low energy dislocation structures to minimize long-range stresses in the crystalline material [21], [22]. The model is able to predict the dislocation density trend during straining shown in Fig. 4, by the rapid initial increase in parameter N_D. N_D varies by orders of magnitude from $10^{10}\,\mathrm{m}^{-2}$ in the AR sample (0% strain) to $10^{13}\,\mathrm{m}^{-2}$, after 5% deformation, and $10^{14}\,\mathrm{m}^{-2}$ after 16% deformation. The N_d values of $10^{10}\,\mathrm{m}^{-2}$, for the AR and AR+1000 °C/3 h sample indicate that the EB melted ingot and the 1000 °C/3 h heat treatment have very low starting dislocation densities consistent with fully annealed material [9].

The actual dislocation densities in these samples can only be verified by advanced microscopy such as transmission electron microscopy or high resolution electron back-scatter imaging. The authors want to note here that, the evolution of dislocation density under strain is complex depends on orientation, purity, and initial microstructure- single crystal versus poly-crystalline with grain boundaries [23], and a full description is beyond the scope of this paper. The relationship between shear strain (γ) on the slip system and dislocation density (ρ), burgers vector (b), and dislocation velocity (v) in low strain ($\leq 1\%$) regimes follows the Taylor-Orowan equation [24]. For higher strains, dislocation interactions lead to complex structures and involves sophisticated models for dislocation dynamics to predict dislocation density evolution [25], [26]. In general for annealed single or polycrystalline Nb microstructure, the dislocation density increases at a faster rate during initial stages of plastic deformation and begins to plateau with increase in strain [20], a trend also observed from the estimated dislocation density parameter in Fig. 4. It is speculated that trends observed in this paper maybe applicable to polycrystalline Nb material with very low preferential texture.

B. *Dependence of the Phonon Peak*

In previous studies of measurement of resistivity versus strain [27], there is an appearance of the phonon peak in the undeformed sample and the phonon peak persists up to a strain of 7% for very high RRR Nb, indicating that the decrease in the phonon peak is mainly a contribution of increased dislocation content. However, we do not see any phonon peak in the as-received EB melted sample in this study and only after a 1000 °C/3 h annealing of the undeformed AR sample. Since there is no deformation in the EB melted AR and AR +1000 °C/3 h sample, the dislocation content does not vary in these samples, which is also confirmed by the N_d value of $10^{10}\,\mathrm{m}^{-2}$ provided by the model.

The initial condition of our samples are EDM cut +BCP, which introduces hydrogen and interstitials into the initial sample [28]. After a 1000 °C/3 h in a $< 10^{-6}$ torr environment in the absence of gettering, only hydrogen is removed from the bulk whereas oxygen from the environment diffuses through the bulk. The removal of H leads to the appearance of the phonon peak,

whereas the increase in overall interstitial O content would lead to a decrease in κ, over the temperature range as indicated in Fig. 3 [29]. We would expect the phonon peak in our samples if the study was repeated with samples that were initially annealed with gettering and then strained to introduce dislocations. In fact, what we have shown here indicates a robust model able to predict the dislocation density in spite of other initial condition that can affect the thermal conductivity, in this instance being heat treatment, and interstitial content even in the presence of a phonon peak. These initial experiments show a non-linear dependence of resistivity with strain when the initial material condition is kept constant. Independent resistivity measurements could be preformed to verify this trend.

VI. Summary

The thermal conductivity of large-grain Nb after varying tensile strains has been measured. The fitted thermal conductivity considering phonon scattering by dislocations agrees well with the experimental results. The model is robust and able to predict the dislocation density even in the presence of a phonon peak when there is no deformation. The predicted dislocation density by the model does not vary significantly between EB melted and annealing treatment suggesting that the initial EB melted material has very low dislocation content or internal strain. Preliminary results indicates a non-linear relationship between plastic strain and resistivity, and an expected trend in the evolution of dislocation density that incorporates the stage 1, 2, and 3 hardening behavior typical of cubic metals.

Acknowledgment

The authors acknowledge the help of Korey Getty and the NHMFL machine shop for cutting the EB melted Nb slabs and preparing the tensile samples for this study.

References

[1] S. Belomestnykh et al., "Key directions for research and development of superconducting radio frequency cavities," 2022, *arXiv:2204.01178*.
[2] S. V. Kutsaev et al., "Niobium quarter-wave resonator with the optimized shape for quantum information systems," *EPJ Quantum Technol.*, vol. 7, no. 1, 2020, Art. no. 7, doi: 10.1140/epjqt/s40507-020-00082-8.
[3] H. Padamsee, *RF Superconductivity: Science, Technology, and Applications*. Hoboken, NJ, USA: Wiley, 2009.
[4] H. Padamsee, *Superconducting Radiofrequency Technology for Accelerators: State of the Art and Emerging Trends*. Wiley, 2023.
[5] P. Dhakal, "Nitrogen doping and infusion in SRF cavities: A review," *Phys. Open*, 5, 2020, Art. no. 100034.
[6] A. Grassellino et al., "Unprecedented quality factors at accelerating gradients up to 45 MVm-1 in niobium superconducting resonators via low temperature nitrogen infusion," *Supercond. Sci. Technol.*, vol. 30, no. 9, Aug. 2017, Art. no. 094004, doi: 10.1088/1361-6668/aa7afe.
[7] P. Dhakal, S. Chetri, S. Balachandran, P. J. Lee, and G. Ciovati, "Effect of low temperature baking in nitrogen on the performance of a niobium superconducting radio frequency cavity," *Phys. Rev. Accel. Beams*, vol. 21, no. 3, Mar. 2018, Art. no. 032001, doi: 10.1103/PhysRevAccelBeams.21.032001.
[8] E. M. Lechner, J. W. Angle, F. A. Stevie, M. J. Kelley, C. E. Reece, and A. D. Palczewski, "RF surface resistance tuning of superconducting niobium via thermal diffusion of native oxide," *Appl. Phys. Lett.*, vol. 119, no. 8, Aug. 2021, Art. no. 082601, doi: 10.1063/5.0059464.
[9] T. R. Bieler et al., "Physical and mechanical metallurgy of high purity Nb for accelerator cavities," *Phys. Rev. Spec. Top. - Accel. Beams*, vol. 13, no. 3, Mar. 2010, Art. no. 031002, doi: 10.1103/PhysRevSTAB.13.031002.
[10] D. Kang, T. R. Bieler, and C. Compton, "Effects of processing history on the evolution of surface damage layer and dislocation substructure in large grain niobium cavities," *Phys. Rev. Special Top. - Accel. Beams*, vol. 18, no. 12, Dec. 2015, Art. no. 123501, doi: 10.1103/PhysRevSTAB.18.123501.
[11] P. Xu, T. Bieler, and N. Wright, "Effect of dislocations on the thermal conductivity of superconducting Nb," in *Proc. 18th Int. Conf. RF Supercond.*, 2017, pp. 886–890, doi: 10.18429/JACOW-SRF2017-THPB061.
[12] P. Xu, "Investigation of the Thermal Transport in Superconducting Niobium and Tantalum," Ph.D. dissertation, Dept. Mech. Eng., Michigan State Univ., East Lansing, MI, USA, 2019.
[13] "Standard test methods for tension testing of metallic materials," 2022. Accessed: Nov. 09, 2022. [Online]. Available: https://www.astm.org/e0008e0008m-22.html
[14] G. Ciovati, P. Dhakal, I. Parajuli, T. Saeki, and M. Walive Pathiranage, "Thermal conductivity of electroplated Copper onto bulk Niobium at cryogenic temperatures," in *Proc. 20th Int. Conf. RF Supercond.*, 2022, pp. 576–580, doi: 10.18429/JACOW-SRF2021-WEPFDV008.
[15] J. Bardeen, G. Rickayzen, and L. Tewordt, "Theory of the thermal conductivity of superconductors," *Phys. Rev.*, vol. 113, no. 4, pp. 982–994, Feb. 1959, doi: 10.1103/PhysRev.113.982.
[16] F. Koechlin and B. Bonin, "Parametrization of the niobium thermal conductivity in the superconducting state," *Supercond. Sci. Technol.*, vol. 9, no. 6, Jun. 1996, Art. no. 453, doi: 10.1088/0953-2048/9/6/003.
[17] J. Bardeen, L. N. Cooper, and J. R. Schrieffer, "Theory of Superconductivity," *Phys. Rev.*, vol. 108, no. 5, pp. 1175–1204, Dec. 1957, doi: 10.1103/PhysRev.108.1175.
[18] P. G. Klemens, "The scattering of low-frequency lattice waves by static imperfections," *Proc. Phys. Soc. Sect. A*, vol. 68, no. 12, Dec. 1955, Art. no. 1113, doi: 10.1088/0370-1298/68/12/303.
[19] R. B. Zubeck, T. W. Barbee Jr, T. H. Geballe, and F. Chilton, "Effects of plastic deformation on the superconducting specific-heat transition of niobium," *J. Appl. Phys.*, 50, 1979, Art. no. 6423.
[20] R. W. K. Honeycombe, *The Plastic Deformation of Metals*, 2nd ed. London, U.K.: Edward Arnold Ltd., 1984.
[21] J. G. Sevillano and E. Aernoudt, "Low energy dislocation structures in highly deformed materials," *Mater. Sci. Eng.*, vol. 86, pp. 35–51, Feb. 1987, doi: 10.1016/0025-5416(87)90441-1.
[22] D. Kuhlmann-Wilsdorf, "LEDS: Properties and effects of low energy dislocation structures," *Mater. Sci. Eng.*, vol. 86, pp. 53–66, Feb. 1987, doi: 10.1016/0025-5416(87)90442-3.
[23] N. Hansen, "Cold deformation microstructures," *Mater. Sci. Technol.*, vol. 6, pp. 1039–1047, 1990.
[24] E. Orowan, "Problems of plastic gliding," *Proc. Phys. Soc.*, 52, 1940, Art. no. 8.
[25] H. Zbib, T. De La Rubia, M. Rhee, and J. Hirth, "3D dislocation dynamics: Stress-strain behavior and hardening mechanisms in FCC and BCC metals," *J. Nucl. Mater.*. 276, pp. 154–165, 2000.
[26] E. P. Kulyadi, "Investigating single crystal plasticity of niobium with a dislocation mechanics-based model," Ph.D. dissertation, Dept. Mater. Sci. Eng., Michigan State Univ., East Lansing, MI, USA, 2022.
[27] W. Wasserbäch, "Low-temperature thermal conductivity of pure and impure niobium and tantalum single crystals," *Physica Status Solidi (B)*, vol. 84, no. 1, pp. 205–214, 1977, doi: 10.1002/pssb.2220840123.
[28] S. K. Chandrasekaran, T. R. Bieler, C. Compton, and N. T. Wright, "Hydrogen saturation and the thermal conductivity of superconducting niobium," in *Proc. SRF'13*, 2013, pp. 589–592.
[29] S. K. Chandrasekaran, "Role of metallurgy in the thermal conductivity of superconducting niobium," Ph.D. dissertation, Dept. Mech. Eng., Michigan State Univ., East Lansing, MI, USA, 2013.